Journal of Cellular Biochemistry 90:473–483 (2003)

Molecular Imaging in Prostate Cancer

Jose A. Karam,[1] Ralph P. Mason,[2] Kenneth S. Koeneman,[1] Peter P. Antich,[2] Elie A. Benaim,[1] and Jer-Tsong Hsieh[1]*

[1]Department of Urology, University of Texas Southwestern Medical Center at Dallas, Dallas, Texas
[2]Department of Radiology, University of Texas Southwestern Medical Center at Dallas, Dallas, Texas

Abstract Prostate cancer (PCa) is the most common non-cutaneous malignancy in men. New ways to diagnose this cancer in its early stages are needed. Unique genetic and biochemical changes in the cell pave the way for tumors to grow and metastasize. Novel imaging approaches attempt to detect pathological processes in cancer cells at the molecular level. This has led to the establishment and development of the field of molecular imaging. Positron emission tomography (PET), magnetic resonance spectroscopic imaging (MRSI), magnetic resonance imaging (MRI), and radiolabeled antibodies are a few of the modalities that can detect abnormal tumor metabolic processes in the clinical setting. Other imaging techniques are still in their early phase of development but hold promise for the future, including bioluminescence imaging (BLI), measurement of tumor oxygenation, and measurement of uptake of iodine by tumors. These techniques are non-invasive and can spare the patient undue morbidity, while potentially providing early diagnosis, accurate follow-up and, finally, valuable prognostic information. J. Cell. Biochem. 90: 473–483, 2003.

Key words: molecular imaging; prostate cancer; PET; MRI; bioluminescence; tumor oximetry; radiolabeled antibodies

American Cancer Society, Cancer Facts and Figures [2003] estimates that 220,900 men will be diagnosed with prostate cancer (PCa) and 28,900 will die from the disease. Conventional imaging studies such as ultrasound, CT scans, radiographs, and magnetic resonance imaging (MRI) have played a rather limited role in the diagnosis, staging, and monitoring of patients with PCa. For example, transrectal ultrasound (TRUS) is routinely used to perform prostate biopsies; unfortunately, PCa can be isoechoic and indistinguishable from the surrounding normal prostate tissue [Norberg et al., 1997]. Likewise, up to 40% of patients undergoing radical prostatectomy for presumed clinically organ-confined disease are found to have extra-prostatic extension upon further pathologic staging [Epstein et al., 1996]. These patients are unlikely to benefit from surgery, but they will be exposed to its potential complications, which are significant. Newer, non-invasive imaging techniques need to be developed in order more accurately to diagnose, stage and monitor patients with PCa. Exciting developments in molecular and cellular biology have highlighted the key underlying processes involved in cancer pathogenesis. The parallel evolution of non-invasive imaging has led to what is now known today as molecular imaging. This article reviews various modalities of molecular imaging in PCa.

POSITRON EMISSION TOMOGRAPHY

PET is based on the use of tracers labeled with positron-emitting radioisotopes. These tracers are injected into the circulation, but they localize to specific organs where they are preferentially metabolized by abnormal or cancerous target cells. The tracer emits a positron that annihilates with an electron in the adjacent tissue. This results in two photons that leave the tissue in exactly opposite directions and are detected by photon detectors in the PET scan, allowing for anatomical localization of the

*Correspondence to: Jer-Tsong Hsieh, PhD, Associate Professor of Urology, Department of Urology, University of Texas Southwestern Medical Center at Dallas, 5323 Harry Hines Blvd., Dallas, TX 75390-9110.
E-mail: JT.Hsieh@UTSouthwestern.edu
Received 2 July 2003; Accepted 3 July 2003
DOI 10.1002/jcb.10636

emitted positron. An example of PET imaging following administration of ^{18}F-FDG to a Dunning prostate tumor-bearing rat is shown in Figure 1.

PET scan has been tested in PCa patients prior to initiation of treatment. The most studied radiotracer is ^{18}F-fluorodeoxyglucose (^{18}F-FDG) that accumulates in cancer cells due to elevated glycolysis [Mathews and Oz, 2002]. However, ^{18}F-FDG PET has not been helpful in staging PCa prior to treatment. No correlation was found between tumor grade, stage, and ^{18}F-FDG uptakes by PET [Effert et al., 1996]. In fact, when compared to ultrasound, computer tomography (CT), or MRI, ^{18}FDG-PET did not offer any additional information [Effert et al., 1996].

In addition, ^{18}F-FDG-PET was evaluated for the detection of osseous and soft tissue metastasis of PCa in a study of 34 patients with known or suspected metastasis and was found to have lower sensitivity than conventional radionuclide bone scans [Shreve et al., 1996].

In another study of 45 patients who underwent definitive local therapy for PCa, both PET and CT detected 50% of all distant metastasis in those who had a prostate specific antigen (PSA) level >4. This detection rate, which was superior to that of ^{111}indium (^{111}In) Capromab Pendetide scan [Seltzer et al., 1999], suggests that combining PET and CT could be useful for detecting distant metastasis in patients with PCa.

Other radiotracers (^{11}C-choline, ^{18}F-choline, ^{18}F-fluoromethylcholine, ^{18}F-fluoroethylcholine (^{18}F-FECh), ^{11}C-acetate) have been studied in PCa. ^{18}F-fluorocholine and ^{11}C-choline have been shown to be actively transported into PCa cells, where they are phosphorylated and

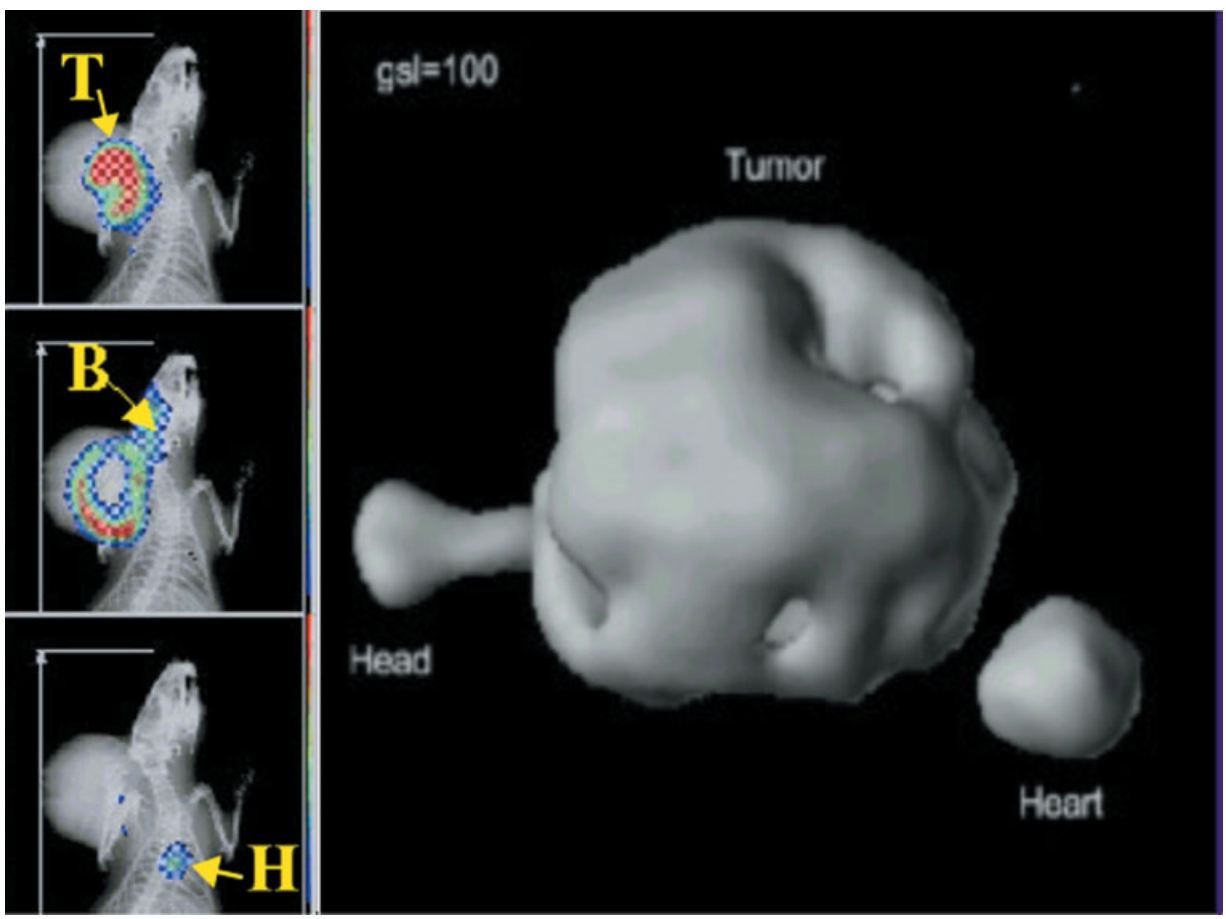

Fig. 1. Positron emission tomography (PET) superimposed on planar X-ray showing tumor (T), brain (B), and heart (H) following administration of ^{18}F-FDG to a rat bearing a Dunning prostate R3327-AT1 pedicle tumor (**left panel**). The **right panel** represents 3-dimensional (3D) reconstruction of the ^{18}F-FDG PET. (Data obtained in association with Drs. Tsyganov, Öz, Constantinescu, McColl.)

sequestered [DeGrado et al., 2001]. Compared to ^{11}C-choline, ^{18}F-FECh has a longer half-life, which allows prolonged storage and transportation and yields a higher resolution on PET scan [Hara et al., 2002]. In a recent study, ^{11}C-choline and ^{18}F-FDG PET were compared to CT in 100 patients for restaging PCa after radical prostatectomy (77 patients) or radiotherapy (23 patients). On three occasions, restaging was done when recurrence or metastasis was suggested due to a rising PSA. Areas of abnormal uptake were 47% for ^{11}C-choline as compared to 27% for ^{18}F-FDG. Areas of abnormal density were detected in 49% of patients on CT. The agreement between ^{11}C-choline and ^{18}F-FDG was 86%. ^{11}C-choline seems to be better than ^{18}F-FDG in restaging PCa after radical therapy; however, ^{11}C-Choline PET scan should be used as complementary to conventional imaging such as CT [Picchio et al., 2003]. ^{11}C-acetate PET was compared to ^{18}F-FDG PET in a study of 22 patients with PCa. All 22 patients had PCa as proven by TRUS-guided prostate biopsy, but only five patients eventually underwent radical prostatectomy and lymph node (LN) dissection. Seven bone metastases were detected by ^{99}Tc bone scintigraphy. ^{11}C-acetate PET detected 100% of primary prostate lesions, 100% of LN metastasis, and 86% of bony metastasis, while ^{18}F-FDG PET only detected 83, 40, and 57%, respectively [Oyama et al., 2002]. The role of PET scan in patients with PCa is still evolving. At this point, its main value appears to be in the detection of tumor recurrence and/or progression after radical local therapy. The use of the novel PET tracers in randomized prospective trials in the future is warranted to determine the ultimate role of PET in the diagnosis, staging, and monitoring of patients with PCa.

Recently, PET has been tested for its ability to image adenoviral-HSV-thymidine kinase (*TK*) gene expression in severe combined immunodeficient (SCID) mice carrying human PCa cells. Mice were serially injected with ^{18}F-FDG and ^{18}F-fluoropenciclovir. All tumor xenografts were easily imaged with ^{18}F-FDG. However, only tumors that were transfected with the adenovirus bearing *TK* gene showed signal with ^{18}F-fluoropenciclovir PET [Pantuck et al., 2002]. This preclinical model demonstrates that this technique could potentially be used to image and monitor the effects of gene therapy in the prostate [Freytag et al., 2001]. However, further experiments are needed to determine if there is a differential uptake of the adenovirus by normal and cancerous tissues. After appropriate validation in the animal model, human studies should be instituted to study both the safety and reliability of PET-gene imaging.

Overall, PET is most widely used in conjunction with ^{18}F-FDG, which is a well-established indicator of metabolic activity. However, in the case of PCa, the variable metabolic rate makes PET less definitive diagnostically. Newer agents are under development including ^{18}FLT (^{18}F-3′-deoxy-3′-fluorothymidine) as an indicator of mitosis and proliferation [Shields et al., 1998], ^{64}Cu-ATSM (copper-diacetyl-bis-*N*4-methylthiosemicarbazone) for hypoxia [Lewis et al., 1999], and ^{64}Cu-PTSM (copper-64-pyruvaldehyde-bis-*N*4-methylthiosemicarbazone) for blood flow [Flower et al., 2001]. These additional agents promise greater sensitivity and specificity, and they can potentially provide more insight into pathobiological characteristics of PCa.

MAGNETIC RESONANCE SPECTROSCOPIC IMAGING (MRSI)

MRSI is a tool that combines magnetic resonance and spectroscopy to yield 3-dimensional (3D) anatomic information with concurrent delineation of metabolic processes.

MRSI can detect several different metabolites in the prostate, whose levels are altered in PCa. Choline levels increase and citrate levels decrease in PCa when compared to benign prostatic hyperplasia (BPH) and normal peripheral zone tissues [Kurhanewicz et al., 1996].

Spectroscopy has shown that levels of the polyamine spermine (a putative inhibitor of PCa development) are very low in human PCa tissue, and this result is validated by histopathology [Cheng et al., 2001]. Decreased spermine levels are seen in PCa, especially when metastasis is present, as compared to normal tissue and BPH [Van Der Graaf et al., 2000].

In a prospective study, the ability of 3D-MRSI to detect residual or recurrent disease was tested in 25 patients with PCa after treatment with primary cryotherapy. Based on citrate, creatine, and choline measurement, 3D-MRSI was able to detect more foci of PCa than MRI, TRUS, and TRUS-guided biopsy [Parivar et al., 1996]. In a study comparing the use of MRI and 3D-MRSI, the combination of MRI and

spectroscopic imaging findings was more predictive (positive predictive value of 89–92%) and specific (91% specificity) in detecting PCa than either modality alone. In this study, the absence of findings suggestive of PCa on either MRI or spectroscopy almost completely excluded the possibility of PCa [Scheidler et al., 1999]. When combined, endorectal MRI and spectroscopy also resulted in a statistically significant improvement in the detection of extracapsular extension of PCa even when an inexperienced radiologist interpreted the images [Yu et al., 1999].

However, the use of MRI/3D-MRSI is still limited to a few centers where this technology is available. Future multicenter prospective trials comparing this new imaging technology to conventional imaging are needed to understand its clinical usefulness in the field of urologic oncology. As shown in a representative normal human prostate in Figure 2, there is considerable heterogeneity in the signals generated. The use of newer metabolic markers like spermine may potentially provide a more sensitive and accurate imaging of disease recurrence or progression. Finally, increasing the magnetic field strength in future MR scanners and obtaining a better signal-to-noise ratio with potentially smaller voxels should help in identifying more specific and accurate markers.

MAGNETIC RESONANCE IMAGING

The role of MRI in the diagnosis, staging and monitoring of patients with PCa is still evolving. PCa is best detected on T2 weighed MRI as discrete areas of low intensity surrounded by a high signal intensity area from the surrounding benign tissue. However, this observation is mainly applicable to tumors larger than 5 mm [Ellis et al., 1994]. MRI can reveal exquisite anatomical details (Fig. 2), but the images need to be interpreted with caution due the signal drop associated with endorectal coils.

A new method called diffusion-weighted MRI (DWI) is based on the fact that the motion of water in human tissues is affected by barriers like cell membranes, and thus, DWI can detect changes in cellular structure and integrity. DWI utilizes a tumor behavior termed "apparent diffusivity" to detect tumor cells from normal tissue. This property is quantitated by the apparent diffusivity coefficient, ADC. This new technique has been studied in a transgenic

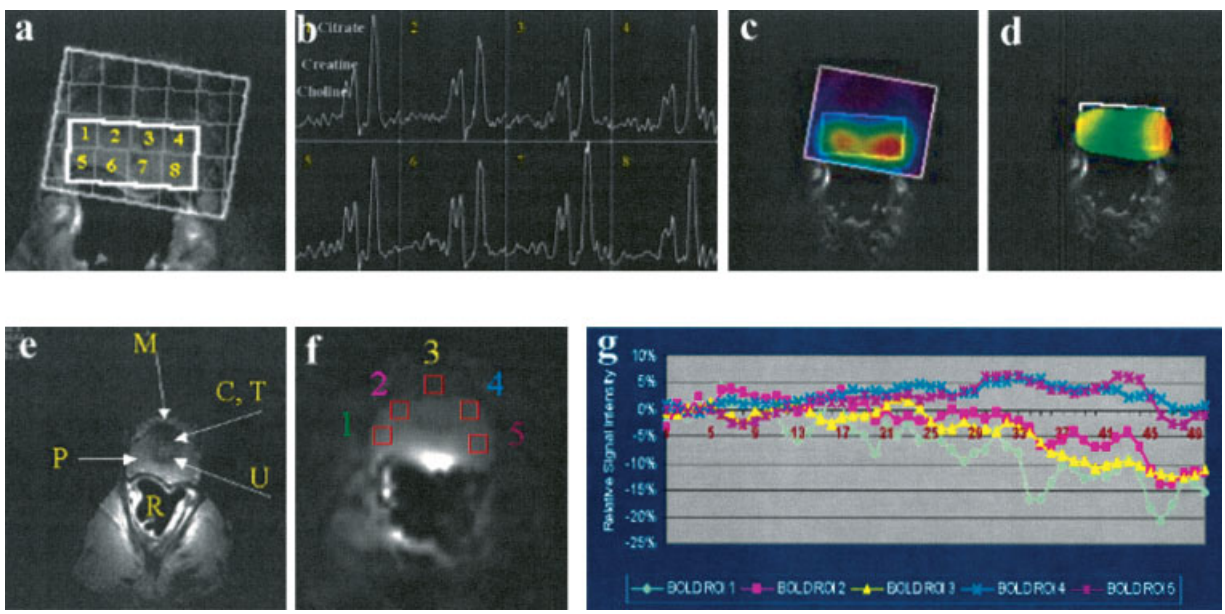

Fig. 2. Magnetic resonance (MR). (**a**) shows normal conventional magnetic resonance imaging (MRI) with a spectral display grid. (**b**) shows the levels of citrate, choline, and creatine in different areas of a normal prostate. (**c** and **d**) are MRS with citrate and citrate/choline metabolic maps, respectively. (**e**) MRI from a healthy volunteer depicting normal anatomy (T, transitional zone; P, peripheral zone; U, urethra; R, rectum; C, central zone; M, muscle) Blood Oxygenation Level Dependent (BOLD) MRI. (**g**) shows the response of five prostate regions (labeled in (**f**)) following O_2 breathing. (Data obtained in association with Lan Jiang and Drs. Nurenberg and Dr. Metzger.)

mouse model of PCa CR2-TAg. Recent data indicates that the tumor-to-normal tissue contrast is enhanced in DWI as compared to regular T2 weighted images. Often, tightly packed glandular elements are present in PCa, resulting in increased resistance to water motion, which cannot be clearly resolved by regular T2 weighted imaging. In contrast, DWI utilizes tissue water diffusion characteristics to yield better tumor-to-normal tissue delineation [Song et al., 2002].

In another study, where MRI was used for prostate-specific imaging, gadolinium (Gd^{3+}) was bound to a nucleus-localizing module, resulting in a cell nucleus-directed nuclear localization sequence–Gd^{3+} complex (CNN–Gd^{3+}-complex). DU-145 cells (an androgen-independent [AI] PCa line) were incubated with this complex and visualized using MRI and laser confocal scanning microscopy (LCSM). MRI visualized the complex uptake by the DU-145 cells; however, nuclear localization could not be ascertained by this method. The presence of the CNN–Gd^{3+}-complex in the intranuclear space was corroborated using LCSM. Gd^{3+} has a large neutron capture cross-section that causes irreversible DNA damage after neutron irradiation. Consequently, Gd^{3+}–CNN could be detected with MRI and used to monitor patients receiving neutron capture therapy [Heckl et al., 2002].

Most recently, a group of investigators used MRI to image clinically occult lymph-node metastasis in patients with PCa after intravenous injection of lymphotropic superparamagnetic nanoparticles containing iron oxide. Eighty patients were enrolled, and 334 LNs were evaluated by imaging and then by histopathology after surgical resection. MRI with nanoparticles correctly identified 100% of patients with metastasis and 90.5% of LNs with metastasis compared to 45.4 and 35.4%, respectively, with conventional MRI. MRI with nanoparticles accurately identified 95.7% of the patients without metastasis and 97.5% of the normal LNs. In contrast, conventional MRI correctly identified 78.7% of patients without regional metastasis and 90.4% non-metastatic LNs. When lymphotropic nanoparticles are used with MRI, LN metastatic foci as small as 2 mm in otherwise normal-size LNs can occasionally be identified. This is well below the sensitivity of conventional MRI and PET [Harisinghani et al., 2003].

Two other MRI-based imaging techniques with potential applications in patients with urologic malignancies are blood oxygenation level dependent (BOLD) MRI and dynamic contrast enhanced (DCE) MRI. BOLD MRI is based on the ability of T2 weighted MRI to differentiate between deoxyhemoglobin and oxyhemoglobin after inhalation of 100% oxygen (O_2) or carbogen (5% CO_2 and 95% O_2 mixture). This technique could delineate areas of malignancy, which are characteristically hypooxygenated [Taylor et al., 2001]. An example of BOLD MRI in a normal human prostate is shown in Figure 2. It is worth noting that some signals decrease with elevated oxygen breathing, suggesting a "steal effect." DCE MRI works by detecting Gd^{3+} complexes to evaluate tumor physiology-specifically tumor blood volume, tumor perfusion and vessel permeability [Barentsz et al., 1999]. These MRI techniques have the potential to simultaneously provide valuable functional and anatomical information and may be available in the future after appropriate testing in animal models and humans.

PROSTATE SPECIFIC MEMBRANE ANTIGEN (PSMA)

PSMA is a type II membrane glycoprotein localized on the membrane of prostatic cells [Grauer et al., 1998]. PSMA has been found in benign prostate, prostatic intraepithelial neoplasia, and PCa, but its level of expression is much higher and homogenous in cancer, especially in higher-grade tumors [Bostwick et al., 1998]. PSMA was also detected in 98% of LN metastasis from PCa [Sweat et al., 1998].

An antibody for the internal domain of PSMA ($PSMA_{int}$) was developed (7E11-C5.3) and conjugated with ^{111}In. Injection into patients with PCa demonstrated the in vivo expression of PSMA. This technology (ProstaScint™, or Capromab Pendetide) is currently limited to patients with clinically localized PCa at high risk for positive LNs and in patients after radical prostatectomy in which recurrence or metastasis is suspected [Rosenthal et al., 2001]. Recently, a multicenter retrospective study evaluated ProstaScint in 255 patients with early evidence of biochemical recurrence after radical prostatectomy. In this study, 72% of the patients had a positive scan. Prostatic fossa uptake occurred in 30.6% of these patients, while

regional uptake and distant uptake occurred in 42.8 and 29.4% of the patients, respectively. The serum PSA level did not correlate with the site of disease recurrence. This study concluded that ProstaScint could detect and localize early biochemical recurrences after radical prostatectomy without a minimum PSA level [Raj et al., 2002].

The finding that the antibody 7E11-C5.3 can bind only to $PSMA_{int}$, which is mainly accessible when the tumor cells are apoptotic or necrotic, has led to the development of an antibody against the external domain of PSMA ($PSMA_{ext}$) [Liu et al., 1997]. Recently, the radiolabeled forms of this antibody (^{111}In-J591 and ^{131}I-J591) were studied in nude mice bearing PCa xenografts and compared to ^{111}In-7E11-C5.3 in terms of pharmacokinetics and tumor uptake. ^{131}I-J591 antibodies were taken up 20 times more in PSMA-positive tumors than in PSMA-negative tumors. In addition, the clearance of ^{131}I-J591 from the circulation was faster than that of ^{111}In-7E11-C5.3, resulting in a larger tumor-to-blood ratio for ^{131}I-J591. Using autoradiography of tumor sections, ^{111}In-7E11-C5.3 was found to be localized in areas of necrosis, while ^{131}I-J591 localized in areas of viable tumors [Smith-Jones et al., 2003]. This may have diagnostic, as well as therapeutic, implications for patients with PCa because richly vascularized areas like LNs and bony metastasis would be more readily accessible with ^{131}I-J591 and ^{111}In-J591, as compared to ^{111}In-7E11-C5.3.

Na-I SYMPORTER (NIS)

NIS is a transmembrane channel that is responsible for the simultaneous transportation of sodium and iodine into the cell, most notably in the thyroid gland from which it was recently cloned [Dai et al., 1996]. The potential application of NIS in PCa was evaluated using a mammalian expression vector expressing human NIS under the control of a PSA promoter. This vector was transfected into LNCaP (androgen-dependent [AD]) and PC-3 cells (AI PCa cell line) to produce stable transfectant cell lines. After addition of iodine to the cells in culture, LNCaP cell lines concentrated ^{125}I about 50-fold as compared to the control cell lines. This uptake was AD and perchlorate-sensitive (perchlorate is a chemical that inhibits iodide transport). In contrast, PC-3 did not show any perchlorate-sensitive iodide uptake since it does not express PSA [Spitzweg et al., 1999].

The in vivo application of the cloned human *NIS* gene was also evaluated. LNCaP cells were stably transfected with the hNIS-expressing vectors, and xenografts were established in nude athymic mice. This was followed by ^{123}I injection and visualization using a gamma camera. The NIS-transfected LNCaP-containing mice showed up to 30% accumulation of the radioiodine dose administered. In contrast, there was no uptake in the control group. Then, ^{131}I was injected in mice bearing the tumor with NIS, with saline injections as negative controls. All tumors showed more than 50% decrease in size, with some tumors becoming undetectable. Notably, none of the mice demonstrated any adverse side effects to radioiodine therapy [Spitzweg et al., 2000].

The use of iodine in imaging and treatment of disease is a relatively old modality used in thyroid diseases. The appeal of the newer technology is that iodine, a metabolite normally found in the body, could be used to image and treat cancers that uptake iodine. Suitable conditions are needed to keep the radioiodine inside the cell for a period long enough to exert its therapeutic effect [Haberkorn, 2001]. One potential drawback is that the normal thyroid would be affected by the radioactive iodine treatment, and ways to overcome this problem must be formulated before applying it to patients with non-thyroid malignancies. Interestingly, ^{99m}Tc-pertechnetate is also taken up by this transporter [Van Sande et al., 2003], and since this agent is in routine clinical use for nuclear imaging, it promises early application for assessing activity of the NIS reporter gene in clinical practice.

BIOLUMINESCENCE

Recently, the field of bioluminescence imaging (BLI) has been studied in urologic oncology. Nude mice were injected with luciferase-expressing PCa cells either intramuscularly or orthotopically in the prostate. Luciferin (the substrate of luciferase) was then injected, and imaging was performed using an intensified charge coupled device (ICCD). This device detects the photons produced by the interaction between luciferin and luciferase, which are emitted through the skin (Fig. 3). Subsequently, tissue from the mice was harvested and assayed for luciferase activity in vitro. BLI detected a

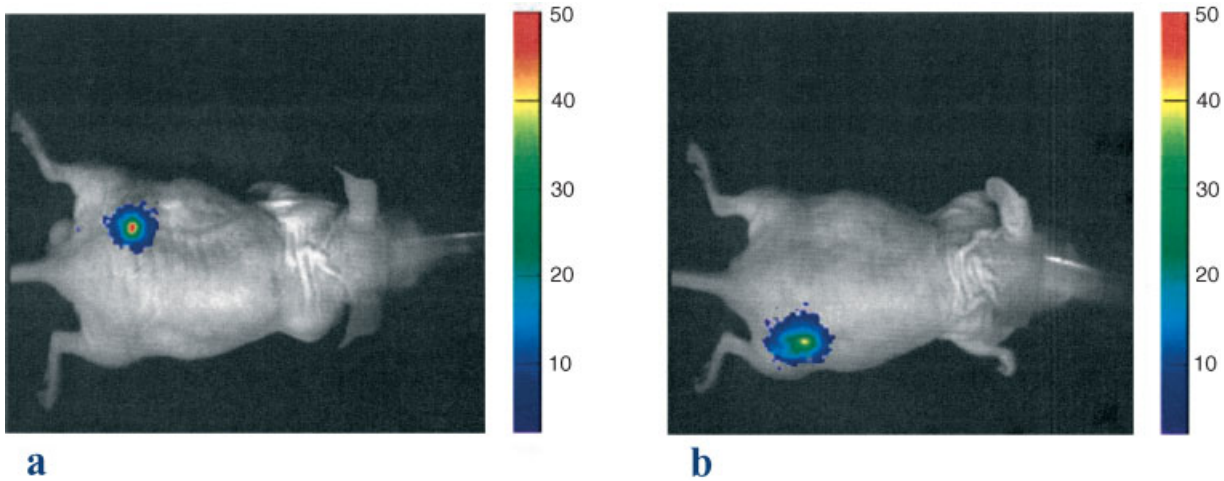

Fig. 3. Bioluminescence imaging (BLI). (**a**, **b**) represent detection of luciferase activity from PC3-luc cells implanted subcutaneously in mice. (Data obtained in association with Robert Bollinger and Dr. R. Gerard, Dr. E. Richer.)

tumor lesion in the thigh at 4 weeks, before any palpable tumor could be identified. After 2 weeks, distinct light emitting areas were detected in the pelvis. Using a luminometric assay, El Hilali et al. [2002] confirmed that these areas represented metastatic pelvic LNs. At 16 weeks, BLI also showed light emission from the prostate and thorax; the latter proved to be a metastatic LN.

In another elegant study, which has demonstrated a potential application of optical imaging in PCa, an adenoviral vector containing the luciferase (*luc*) gene under control of a PSA promoter (AdPSE-BC-luc) was constructed. The vector was injected in SCID mice bearing human PCa tumor xenografts. BLI documented the presence of luciferase activity in the mouse prostate and the human PCa xenograft, with minimal extra-prostatic activity. Luciferase activity was found to correlate with the endogenous PSA level in vivo, but not with the tumor volume. Furthermore, the expression of AdPSE-BC-luc in PCa cells in vitro correlated with PSA and androgen receptor (AR) levels after addition of the androgen analogue R1881 to the cultured cells. Interestingly, the PSA-driven luciferase gene activity was found to be ten times higher in AI prostate tumors, compared to AD tumors [Adams et al., 2002]. Examples of BLI in mice are shown in Figure 3 (male mice were injected with PC3-luciferase cells subcutaneously, and intraperitoneal injection of luciferin revealed the location of the cells, although there was no palpable tumor). In addition to showing the specific luciferase activity in the prostate cells this study also demonstrated the potential to detect minute amounts of luciferase activity in extra-prostatic tissues, namely, the lung and spine, which can be useful when looking for metastasis in patients with PCa. The future use of this technology in humans may help the urologist in directing patient treatment based on the finding of metastatic lesions that cannot be detected by conventional imaging.

TUMOR OXIMETRY

It is known that hypoxic cells resist radiotherapy. Several studies have shown hypoxic regions in human prostate tumors using oxygen electrodes. This could suggest a need for higher radiation doses. However, increased radiation may lead to higher patient morbidity. Therefore, identifying the hypoxic foci could lead to a more focused radiotherapeutic regimen. Based on this need, models to assess tumor oxygenation were developed. It was discovered that an inverse relationship existed between the ^{19}F spin-lattice relaxation rate of perfluorocarbons (PFC) and pO_2, and this relationship has been exploited to study tissue oxygenation status [Mason, 1994].

In early studies, PFC emulsion was injected into tumor-bearing rats intravenously. As PFC cleared from the vasculature, it became sequestered in the tumor, acting as a reporter molecule for O_2. Uptake was highly heterogeneous, particularly in the well-perfused periphery of Dunning R3327-AT1 PCa implanted

subcutaneously on the backs of Copenhagen rats. As the tumors grew, the PFC was retained and revealed progressive hypoxia [Mason et al., 1994]. More recently, hexafluorobenzene (HFB) was identified and found to have preferential characteristics as a reporter molecule, as it has a single resonance providing optimal MR sensitivity and a spin-lattice relaxometric rate that is highly sensitive to O_2, while being minimally responsive to temperature. This technique was termed ^{19}F-nuclear magnetic resonance echo planar imaging relaxometry (FREDOM). HFB was injected into the tumor, both centrally and peripherally. Following traditional imaging, ^{19}F pulse burst saturation recovery echo planar imaging (EPI) relaxometry of HFB was performed. Maps of oxygen partial pressure (pO_2) were obtained and showed heterogeneity in the O_2 distribution inside the tumor tissue [Le et al., 1997]. Several studies in the anaplastic R3327-AT1 PCa lines have revealed heterogeneity with greater hypoxia in larger tumors. Interestingly, once the FiO_2 is increased to 100%, areas that had initially a low pO_2 did not show a significant increase in the pO_2 after oxygenation, whereas areas with a high initial pO_2 showed a marked increase in pO_2 [Mason et al., 1998].

A further study was done to compare cancer cell oxygenation among two PCa lines with different biological behavior. The first model had implantation of a fast growing, highly metastatic MAT-Lu cell line, while the second model had implantation of a slow growing, moderately well differentiated HI cell line. Both sublines exhibited higher oxygenation in smaller tumors than in larger tumors. Respiratory challenge with 100% O_2 resulted in a significant increase in the mean O_2 in both sublines. However, the regions with a low initial O_2 level responded differently to the oxygen challenge, with the HI tumors responding quickly with a significant increase in pO_2, while the metastatic MAT-Lu showed minimal response to 100% O_2 [Zhao et al., 2002]. Examples of differential response to hyperoxic gas inhalation are shown for Dunning prostate R3327 AT1 and HI tumors in Figure 4.

Most significantly, a prognostic value for pO_2 measurements before irradiation in the moderately well differentiated Dunning PCa R3327-

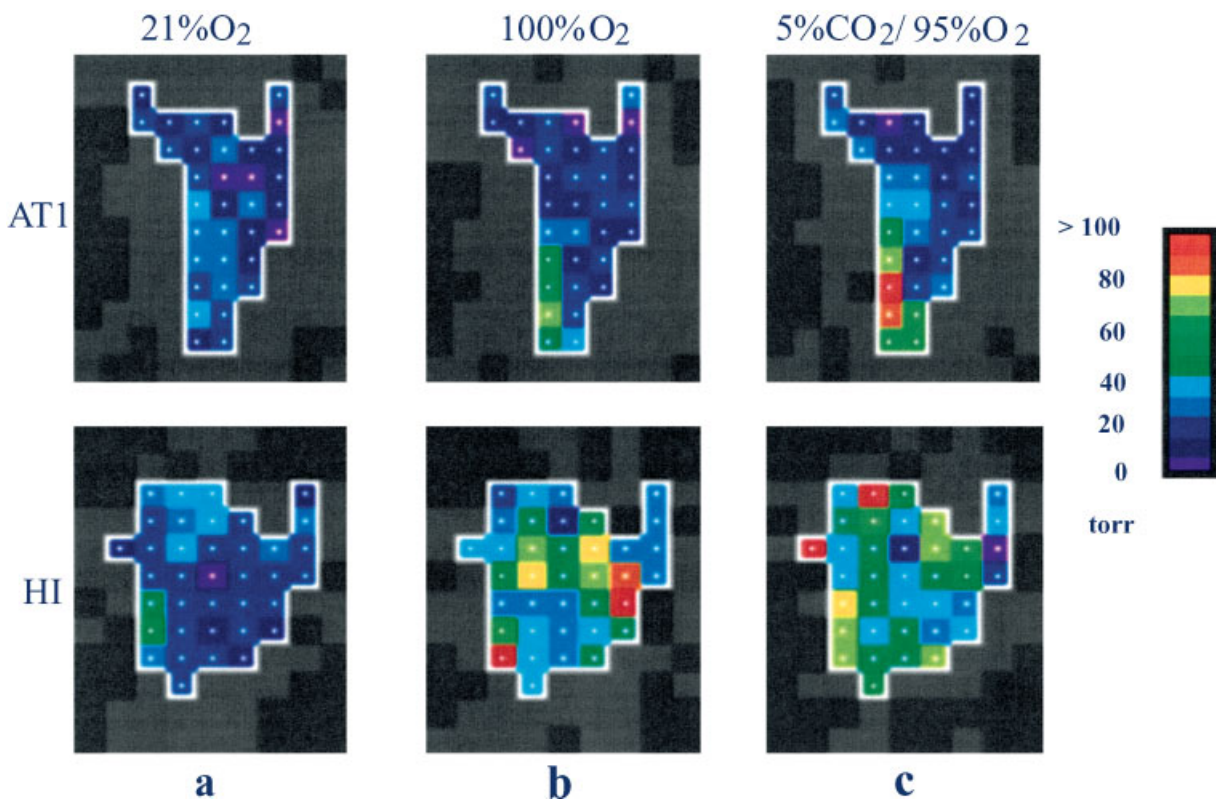

Fig. 4. Tumor oximetry. Oxygen maps (^{19}F-nuclear magnetic resonance echo planar imaging relaxometry, FREDOM) representing Dunning prostate R3327 (AT1 and HI) tumors showing different regional response to breathing hyperoxic gas. (Modified from Zhao et al. [2002].)

HI was demonstrated recently [Zhao et al., 2003]. Irradiation of large tumors (>3.5 cm^3) with 30 Gy single dose while breathing ambient air produced a barely significant tumor growth delay. This ineffectiveness was attributed to extensive tumor hypoxia. By contrast, a separate cohort of rats breathing oxygen showed a significant tumor growth delay, which corresponded with the effective elimination of the hypoxic fraction in this tumor type by oxygen breathing. Interestingly, irradiation of smaller tumors (<2 cm^3) produced significant tumor growth delay irrespective of the inhaled gas (no difference between breathing ambient air and oxygen), which may be attributed to the lack of baseline hypoxia [Zhao et al., 2003].

The potential application of FREDOM to the clinical management of PCa patients should be evaluated in the near future. If the investigations can be translated to the clinic, patient therapy may be individualized based on the degree of tumor hypoxia, and then patients can then be stratified according to their response to intervention.

CONCLUSIONS

Modern imaging techniques have evolved from gross anatomic images to molecular based images. Target molecules include membrane proteins or receptors, reporter molecules, unique metabolites, and ion channels. With such unique features, imaging techniques become an integral part of the modern therapeutic regimen, since the concept of cancer gene therapy is to develop delivery systems and specific targets to eradicate cancer lesions only. However, each cancer type has its own biologic and biochemical signature [Scheffold et al., 2002]; integration and/or development of suitable imaging tools into an effective cancer gene therapy regimen will become a major issue for molecular therapy [Contag and Bachmann, 2002; Edinger et al., 2002]. Since molecular imaging can localize target cells or tissues precisely, it can be used for tracing cancer cells to assess invasion, metastasis pattern, and interaction with adjacent environment in a real-time manner. Moreover, combined with molecular biologic techniques such as DNA array or proteomics, target cells or tissues isolated from a host assisted by molecular imaging may lead to potential gene discovery for disease progression. Similar approaches can be applied on studying drug resistance of cancer cells. Exploring novel molecular targets and developing new tools for imaging will certainly bring researchers close to the goal of PCa cure.

ACKNOWLEDGMENTS

This publication is supported in part by grant National Institute of Health (NIH) P20 CA 086354. We thank Ryan Roark for excellent editorial assistance.

REFERENCES

Adams JY, Johnson M, Sato M, Berger F, Gambhir SS, Carey M, Iruela-Arispe ML, Wu L. 2002. Visualization of advanced human prostate cancer lesions in living mice by a targeted gene transfer vector and optical imaging. Nat Med 8:891–897.

American Cancer Society, Cancer Facts and Figures. 2003. www.cancer.org

Barentsz JO, Engelbrecht M, Jager GJ, Witjes JA, de LaRosette J, van Der Sanden BP, Huisman HJ, Heerschap A. 1999. Fast dynamic gadolinium-enhanced MR imaging of urinary bladder and prostate cancer. J Magn Reson Imaging 10:295–304.

Bostwick DG, Pacelli A, Blute M, Roche P, Murphy GP. 1998. Prostate specific membrane antigen expression in prostatic intraepithelial neoplasia and adenocarcinoma: A study of 184 cases. Cancer 82:2256–2261.

Cheng LL, Wu C, Smith MR, Gonzalez RG. 2001. Non-destructive quantitation of spermine in human prostate tissue samples using HRMAS ^{1}H NMR spectroscopy at 9.4 T. FEBS Lett 494:112–116.

Contag CH, Bachmann MH. 2002. Advances in in vivo bioluminescence imaging of gene expression. Annu Rev Biomed Eng 4:235–260.

Dai G, Levy O, Carrasco N. 1996. Cloning and characterization of the thyroid iodide transporter. Nature 379: 458–460.

DeGrado TR, Coleman RE, Wang S, Baldwin SW, Orr MD, Robertson CN, Polascik TJ, Price DT. 2001. Synthesis and evaluation of ^{18}F-labeled choline as an oncologic tracer for positron emission tomography: Initial findings in prostate cancer. Cancer Res 61:110–117.

Edinger M, Cao YA, Hornig YS, Jenkins DE, Verneris MR, Bachmann MH, Negrin RS, Contag CH. 2002. Advancing animal models of neoplasia through in vivo bioluminescence imaging. Eur J Cancer 38:2128–2136.

Effert PJ, Bares R, Handt S, Wolff JM, Bull U, Jakse G. 1996. Metabolic imaging of untreated prostate cancer by positron emission tomography with ^{18}fluorine-labeled deoxyglucose. J Urol 155:994–998.

El Hilali N, Rubio N, Martinez-Villacampa M, Blanco J. 2002. Combined noninvasive imaging and luminometric quantification of luciferase-labeled human prostate tumors and metastases. Lab Invest 82:1563–1571.

Ellis JH, Tempany C, Sarin MS, Gatsonis C, Rifkin MD, McNeil BJ. 1994. MR imaging and sonography of early prostatic cancer: Pathologic and imaging features that influence identification and diagnosis. AJR Am J Roentgenol 162:865–872.

Epstein JI, Partin AW, Sauvageot J, Walsh PC. 1996. Prediction of progression following radical prostatectomy. A multivariate analysis of 721 men with long-term follow-up. Am J Surg Pathol 20:286–292.

Flower MA, Zweit J, Hall AD, Burke D, Davies MM, Dworkin MJ, Young HE, Mundy J, Ott RJ, McCready VR, Carnochan P, Allen-Mersh TG. 2001. ^{62}Cu-PTSM and PET used for the assessment of angiotensin II-induced blood flow changes in patients with colorectal liver metastases. Eur J Nucl Med 28:99–103.

Freytag SO, Khil M, Stricker H, Peabody J, Menon M, DePeralta-Venturina M, Nafziger D, Pegg J, Paielli D, Brown S, Barton K, Lu M, Aguilar-Cordova E, Kim JH. 2001. Phase I study of replication-competent adenovirus-mediated double suicide gene therapy for the treatment of locally recurrent prostate cancer. Cancer Res 62:4968–4976.

Grauer LS, Lawler KD, Marignac JL, Kumar A, Goel AS, Wolfert RL. 1998. Identification, purification, and subcellular localization of prostate-specific membrane antigen PSM protein in the LNCaP prostatic carcinoma cell line. Cancer Res 58:4787–4789.

Haberkorn U. 2001. Gene therapy with sodium/iodide symporter in hepatocarcinoma. Exp Clin Endocrinol Diabetes 109:60–62.

Hara T, Kosaka N, Kishi H. 2002. Development of ^{18}F-fluoroethylcholine for cancer imaging with PET: Synthesis, biochemistry, and prostate cancer imaging. J Nucl Med 43:187–199.

Harisinghani MG, Barentsz J, Hahn PF, Deserno WM, Tabatabaei S, van de Kaa CH, de la Rosette J, Weissleder R. 2003. Noninvasive detection of clinically occult lymph-node metastasis in prostate cancer. N Engl J Med 348: 2491–2499.

Heckl S, Debus J, Jenne J, Pipkorn R, Waldeck W, Spring H, Rastert R, von der Lieth CW, Braun K. 2002. CNN-Gd^{3+} enables cell nucleus molecular imaging of prostate cancer cells: The last 600 nm. Cancer Res 62:7018–7024.

Kurhanewicz J, Vigneron DB, Hricak H, Narayan P, Carroll P, Nelson SJ. 1996. Three-dimensional H-1 MR spectroscopic imaging of the in situ human prostate with high (0.24–0.7-cm^3) spatial resolution. Radiology 198: 795–805.

Le D, Mason RP, Hunjan S, Constantinescu A, Barker BR, Antich PP. 1997. Regional tumor oxygen dynamics: ^{19}F PBSR EPI of hexafluorobenzene. Magn Reson Imaging 15:971–981.

Lewis JS, McCarthy DW, McCarthy TJ, Fujibayashi Y, Welch MJ. 1999. Evaluation of ^{64}Cu-ATSM in vitro and in vivo in a hypoxic tumor model. J Nucl Med 40:177–183.

Liu H, Moy P, Kim S, Xia Y, Rajasekaran A, Navarro V, Knudsen B, Bander NH. 1997. Monoclonal antibodies to the extracellular domain of prostate-specific membrane antigen also react with tumor vascular endothelium. Cancer Res 57:3629–3634.

Mason RP. 1994. Non-invasive physiology: ^{19}F NMR of perfluorocarbons. Artif Cells Blood Substit Immobil Biotechnol 22:1141–1153.

Mason RP, Antich PP, Babcock EE, Constantinescu A, Peschke P, Hahn EW. 1994. Non-invasive determination of tumor oxygen tension and local variation with growth. Int J Radiat Oncol Biol Phys 29:95–103.

Mason RP, Hunjan S, Le D, Constantinescu A, Barker BR, Wong PS, Peschke P, Hahn EW, Antich PP. 1998. Regional tumor oxygen tension: Fluorine echo planar imaging of hexafluorobenzene reveals heterogeneity of dynamics. Int J Radiat Oncol Biol Phys 42:747–750.

Mathews D, Oz OK. 2002. Positron emission tomography in prostate and renal cell carcinoma. Current Opinion in Urology 12:381–385.

Norberg M, Egevad L, Holmberg L, Sparen P, Norlen BJ, Busch C. 1997. The sextant protocol for ultrasound-guided core biopsies of the prostate underestimates the presence of cancer. Urology 50:562–566.

Oyama N, Akino H, Kanamaru H, Suzuki Y, Muramoto S, Yonekura Y, Sadato N, Yamamoto K, Okada K. 2002. ^{11}C-acetate PET imaging of prostate cancer. J Nucl Med 43:181–186.

Pantuck AJ, Berger F, Zisman A, Nguyen D, Tso CL, Matherly J, Gambhir SS, Belldegrun AS. 2002. CL1-SR39: A noninvasive molecular imaging model of prostate cancer suicide gene therapy using positron emission tomography. J Urol 168:1193–1198.

Parivar F, Hricak H, Shinohara K, Kurhanewicz J, Vigneron DB, Nelson SJ, Carroll PR. 1996. Detection of locally recurrent prostate cancer after cryosurgery: Evaluation by transrectal ultrasound, magnetic resonance imaging, and three-dimensional proton magnetic resonance spectroscopy. Urology 48:594–599.

Picchio M, Messa C, Landoni C, Gianolli L, Sironi S, Brioschi M, Matarrese M, Matei DV, De Cobelli F, Del Maschio A, Rocco F, Rigatti P, Fazio F. 2003. Value of [^{11}C]choline-positron emission tomography for re-staging prostate cancer: A comparison with [^{18}F]fluorodeoxyglucose-positron emission tomography. J Urol 169:1337–1340.

Raj GV, Partin AW, Polascik TJ. 2002. Clinical utility of indium 111-capromab pendetide immunoscintigraphy in the detection of early, recurrent prostate carcinoma after radical prostatectomy. Cancer 94:987–996.

Rosenthal SA, Haseman MK, Polascik TJ. 2001. Utility of capromab pendetide (ProstaScint) imaging in the management of prostate cancer. Tech Urol 7:27–37.

Scheffold C, Kornacker M, Scheffold YC, Contag CH, Negrin RS. 2002. Visualization of effective tumor targeting by CD8+ natural killer T cells redirected with bispecific antibody F(ab′)(2)HER2xCD3. Cancer Res 62:5785–5791.

Scheidler J, Hricak H, Vigneron DB, Yu KK, Sokolov DL, Huang LR, Zaloudek CJ, Nelson SJ, Carroll PR, Kurhanewicz J. 1999. Prostate cancer: Localization with three-dimensional proton MR spectroscopic imaging-clinicopathologic study. Radiology 213:473–480.

Seltzer MA, Barbaric Z, Belldegrun A, Naitoh J, Dorey F, Phelps ME, Gambhir SS, Hoh CK. 1999. Comparison of helical computerized tomography, positron emission tomography, and monoclonal antibody scans for evaluation of lymph node metastases in patients with prostate specific antigen relapse after treatment for localized prostate cancer. J Urol 162:1322–1328.

Shields AF, Grierson JR, Dohmen BM, Machulla HJ, Stayanoff JC, Lawhorn-Crews JM, Obradovich JE, Muzik O, Mangner TJ. 1998. Imaging proliferation in vivo with [F-18]FLT and positron emission tomography. Nat Med 4:1334–1336.

Shreve PD, Grossman HB, Gross MD, Wahl RL. 1996. Metastatic prostate cancer: Initial findings of PET with 2-deoxy-2-[F-18]fluoro-D-glucose. Radiology 199:751–756.

Smith-Jones PM, Vallabhajosula S, Navarro V, Bastidas D, Goldsmith SJ, Bander NH. 2003. Radiolabeled monoclonal antibodies specific to the extracellular domain of prostate-specific membrane antigen: Preclinical studies in nude mice bearing LNCaP human prostate tumor. J Nucl Med 44:610–617.

Song SK, Qu Z, Garabedian EM, Gordon JI, Milbrandt J, Ackerman JJ. 2002. Improved magnetic resonance imaging detection of prostate cancer in a transgenic mouse model. Cancer Res 62:1555–1558.

Spitzweg C, Zhang S, Bergert ER, Castro MR, McIver B, Heufelder AE, Tindall DJ, Young CY, Morris JC. 1999. Prostate-specific antigen (PSA) promoter-driven androgen-inducible expression of sodium iodide symporter in prostate cancer cell lines. Cancer Res 59:2136–2141.

Spitzweg C, O'Connor MK, Bergert ER, Tindall DJ, Young CY, Morris JC. 2000. Treatment of prostate cancer by radioiodine therapy after tissue-specific expression of the sodium iodide symporter. Cancer Res 60:6526–6530.

Sweat SD, Pacelli A, Murphy GP, Bostwick DG. 1998. Prostate-specific membrane antigen expression is greatest in prostate adenocarcinoma and lymph node metastases. Urology 52:637–640.

Taylor NJ, Baddeley H, Goodchild KA, Powell ME, Thoumine M, Culver LA, Stirling JJ, Saunders MI, Hoskin PJ, Phillips H, Padhani AR, Griffiths JR. 2001. BOLD MRI of human tumor oxygenation during carbogen breathing. J Magn Reson Imaging 14:156–163.

Van Der Graaf M, Schipper RG, Oosterhof GO, Schalken JA, Verhofstad AA, Heerschap A. 2000. Proton MR spectroscopy of prostatic tissue focused on the detection of spermine, a possible biomarker of malignant behavior in prostate cancer. MAGMA 10:153–159.

Van Sande J, Massart C, Beauwens R, Schoutens A, Costagliola S, Dumont JE, Wolff J. 2003. Anion selectivity by the sodium iodide symporter. Endocrinology 144:247–252.

Yu KK, Scheidler J, Hricak H, Vigneron DB, Zaloudek CJ, Males RG, Nelson SJ, Carroll PR, Kurhanewicz J. 1999. Prostate cancer: Prediction of extracapsular extension with endorectal MR imaging and three-dimensional proton MR spectroscopic imaging. Radiology 213:481–488.

Zhao D, Constantinescu A, Hahn EW, Mason RP. 2002. Differential oxygen dynamics in two diverse Dunning prostate R3327 rat tumor sublines (MAT-Lu and HI) with respect to growth and respiratory challenge. Int J Radiat Oncol Biol Phys 53:744–756.

Zhao D, Constantinescu A, Chang CH, Hahn EW, Mason RP. 2003. Correlation of tumor oxygen dynamics with radiation response of the Dunning prostate R3327-HI tumor. Radiat Res 159:621–631.